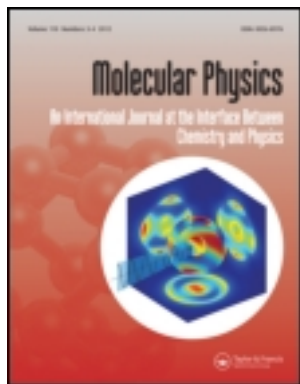


This article was downloaded by: [Emory University]

On: 17 August 2012, At: 07:14

Publisher: Taylor & Francis

Informa Ltd Registered in England and Wales Registered Number: 1072954 Registered office: Mortimer House, 37-41 Mortimer Street, London W1T 3JH, UK



Molecular Physics: An International Journal at the Interface Between Chemistry and Physics

Publication details, including instructions for authors and subscription information:

<http://www.tandfonline.com/loi/tmph20>

Translational energy dependence of the $\text{Cl} + \text{CH}_4(v_b = 0, 1)$ reactions: a joint crossed-beam and quasiclassical trajectory study

Bailin Zhang^a, Kopin Liu^a, Gábor Czakó^b & Joel M. Bowman^b

^a Institute of Atomic and Molecular Science (IAMS), Academia Sinica, P. O. Box 23-166, Taipei 10617, Taiwan

^b Cherry L. Emerson Center for Scientific Computation and Department of Chemistry, Emory University, Atlanta, GA 30322, USA

Accepted author version posted online: 01 Feb 2012. Version of record first published: 21 Feb 2012

To cite this article: Bailin Zhang, Kopin Liu, Gábor Czakó & Joel M. Bowman (2012): Translational energy dependence of the $\text{Cl} + \text{CH}_4(v_b = 0, 1)$ reactions: a joint crossed-beam and quasiclassical trajectory study, *Molecular Physics: An International Journal at the Interface Between Chemistry and Physics*, 110:15-16, 1617-1626

To link to this article: <http://dx.doi.org/10.1080/00268976.2012.662600>

PLEASE SCROLL DOWN FOR ARTICLE

Full terms and conditions of use: <http://www.tandfonline.com/page/terms-and-conditions>

This article may be used for research, teaching, and private study purposes. Any substantial or systematic reproduction, redistribution, reselling, loan, sub-licensing, systematic supply, or distribution in any form to anyone is expressly forbidden.

The publisher does not give any warranty express or implied or make any representation that the contents will be complete or accurate or up to date. The accuracy of any instructions, formulae, and drug doses should be independently verified with primary sources. The publisher shall not be liable for any loss, actions, claims, proceedings, demand, or costs or damages whatsoever or howsoever caused arising directly or indirectly in connection with or arising out of the use of this material.

INVITED ARTICLE

Translational energy dependence of the Cl + CH₄($v_b = 0, 1$) reactions: a joint crossed-beam and quasiclassical trajectory study

Bailin Zhang^{a†}, Kopin Liu^{a*}, Gábor Czakó^b and Joel M. Bowman^b

^aInstitute of Atomic and Molecular Science (IAMS), Academia Sinica, P. O. Box 23-166, Taipei 10617, Taiwan; ^bCherry L. Emerson Center for Scientific Computation and Department of Chemistry, Emory University, Atlanta, GA 30322, USA

(Received 14 December 2011; final version received 24 January 2012)

The Cl + CH₄($v_b = 0, 1$) reactions were studied over a wide range of collision energies, from threshold up to 20 kcal mol⁻¹, using joint experimental and theoretical methods. Experiments were performed under crossed-beam conditions using a time-sliced velocity imaging detection method. Both the pair-correlated integral and differential cross sections were measured. Theoretically, quasiclassical trajectory calculations were performed on a highly accurate *ab initio* potential energy surface. The computed results show very good agreement with experimental findings. The underlying reaction mechanisms are as below: the formation of HCl($v' = 0$) products is mainly governed by direct scatterings, whereas the HCl($v' = 1$) channel is mediated by a time-delayed mechanism, likely invoking reactive resonances. In addition, the spin-orbit excited Cl*(²P_{1/2}) reactivity was experimentally characterized. The results compare favourably with a recently reported reduced dimensionality quantum dynamics calculation, and with the previous reports on the isotopically analogous reactions. Possible involvement of resonances in this spin-orbit nonadiabatic process is suggested and awaits further investigations.

Keywords: time-sliced image; pair-correlated distribution; quasiclassical trajectory; peripheral reaction dynamics

Subject classification codes: chemical dynamics and spectroscopy

1. Introduction

The hydrogen abstraction reaction of the chlorine atom with methane has been extensively studied both experimentally [1–6] and theoretically [7–18] over the past two decades, and is becoming an important proving ground for polyatomic reaction dynamics. In a series of pioneering experiments both Crim's [19–23] and Zare's [24–29] laboratories demonstrated convincingly high mode-specificity as well as bond selectivity in the reactions of chlorine atom with vibrationally excited CH_xD_{4-x}. They found that the rates of reaction depend sensitively on the types of mode excitation, e.g. the differential reactivity of a nearly isoenergetic symmetric-stretching mode of excitation compared to that of the antisymmetric-stretching excitation. In addition, they found preferential cleavage of vibrationally excited bond, and the retention of energy initially deposited in a nonreacting bond during the reaction. On the basis of these observations an intuitively appealing picture emerges: exciting vibrations that resemble the motion along the reaction coordinate can potentially promote the reactivity. More detailed investigations of reactions of

vibrationally excited methane with Cl [6,30–37], F [38–40], and O(³P) [41,42] atoms revealed that the mechanistic origins can be more subtle and complicated. Nonetheless, the above rudimentary concept remains a reasonable picture for guiding our thinking. To gain deeper insights into this fascinating mode- and bond-selective reactivity, it is essential to have the ground-state reaction results at comparable total collision energies as the reaction with vibrationally excited methane because such results serve as a necessary reference to scrutinize the energy requirement for reaction and for comparing the dynamical attributes.

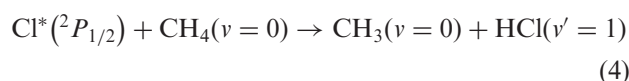
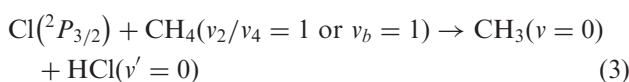
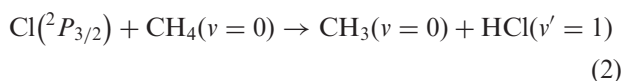
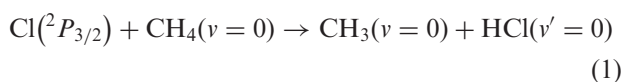
Theoretically, there have been numerous studies of the Cl + CH₄ reaction and its reverse. Duncan and Truong [12] reported a direct *ab initio* dynamics reaction path study of the thermal and vibrationally state-selected rates of this reaction. Several potential energy surfaces (PES) have also been developed and employed in quasiclassical trajectory (QCT) studies and in reduced dimensionality quantum dynamics calculations [7–11,13–16]. In addition, there have been direct dynamics calculations on this system [17]

*Corresponding author. Email: kpliu@gate.sinica.edu.tw

†Present address: Department of Biomedical Engineering, University of Texas at San Antonio, One UTSA Circle, AET 1.240, San Antonio, TX 78249, USA

and calculations of thermal rate constants based on variational transition state theory [18]. While qualitative (or semiquantitative in some cases) comparisons with experimental data could be made, the quantitative agreement was generally lacking. Very recently, a highly accurate PES of this reaction was constructed and the subsequent QCT calculations essentially reproduced most of the available experimental findings [43]. It will be desirable to extend the theory-experiment comparison to higher translational energy regime, which might be more sensitive to the higher energy region of the new PES.

Reported here is a joint experimental and theoretical study on the Cl+CH₄ reaction. Both the integral cross section (ICS) and differential cross-sections (DCS) were measured over a wide range of collision energies, $E_c \sim 2\text{--}20 \text{ kcal mol}^{-1}$, and compared with the QCT results. Specifically we examine the following four state-to-state reactions:



The low energy portion (up to $7.5 \text{ kcal mol}^{-1}$) of experimental data for Reaction (1) that accounts for the major reactivity of Cl+CH₄ are in excellent agreement with the previous report [4]. QCT calculations were performed on the reactions with the ground state Cl(²P_{3/2}) atom, and compared with experimental results. The dynamics of spin-orbit excited Cl*(²P_{1/2}) towards CH₄(*v*=0) are characterized experimentally and compared with theoretical studies in the literature. The remainder of this paper is organized as follows: The experimental approach is briefly given in Section 2, followed by the QCT method in Section 3. The results and discussion are presented in Section 4. Section 5 concludes with a few main points.

2. Experiment

The experiments were conducted using the crossed-beam, ion-imaging apparatus described in detail previously [44,45]. In brief, a pulsed high-voltage

discharge source was used to generate the Cl-atom beam ($\sim 3\%$ Cl₂ seeded in helium at 6 atm.). To achieve high collision energies (E_c), a diluted CH₄ ($\sim 20\%$ CH₄ seeded in H₂ at 6 atm.) was used in this work. By changing the intersection angle of the two molecular beams from 40° to 150°, the entire E_c range of $2.4 \text{ kcal mol}^{-1}$ to $20.4 \text{ kcal mol}^{-1}$ can be covered. The reaction products CH₃ were probed by a (2+1) resonance-enhanced multiphoton ionization (REMPI) scheme via the intermediate 3P_z Rydberg state [46]. The state-tagged product velocity distribution was measured by a time-sliced, velocity imaging technique of the REMPI ions [44]. REMPI spectra of methyl products indicated predominant formation of the vibrational ground state; thus, this report will focus on the pair-correlated dynamics with respect to the CH₃(*v*=0) products.

At a given collision energy, the time-sliced image was acquired with the probe laser frequency fixed at the peak of 0₀⁰ Q-head of the 3P_z²A₂ ← X²A₂ transition. Hence, the product images sampled mostly the low *N*-states of CH₃(*v*=0). Although the vibrationally correlated information could be somewhat biased, this fixed-frequency mode of operation generally yields higher image resolution than an alternative mode that samples all *N*-states by scanning the probe laser frequency over the entire Q-head [6,34]. Since the image resolution was of prime concern for revealing the minor features associated with the reactivity of Cl*(²P_{1/2}) and of the bend excited CH₄(*v*₂/*v*₄=1), we chose to fix the probe laser frequency in this study. Nonetheless, it should be kept in mind when comparing the experimental results thus deduced with the theoretical calculations. To normalize the images at different collision energies for obtaining the reactive excitation function, the procedure described elsewhere [47] was followed in separate measurements.

3. Computational details

QCT calculations of the Cl(²P_{3/2}) + CH₄(*v*=0) as well as the Cl(²P_{3/2}) + CH₄(*v*_{*b*}=1) [*b*=4, 2] reactions were performed using a recently developed, *ab initio*, full-dimensional, spin-orbit ground-state potential energy surface (PES). Detailed description of the PES was reported in [43,62]. We employed standard normal mode sampling [48,49] to prepare the quasiclassical vibrational ground state (*v*=0) and the excited bending states [*v*₄(*t*₂) and *v*₂(*e*)] of CH₄. Small adjustments to the velocities were done to set the total angular momentum of CH₄ to zero. The orientation of CH₄ was randomly rotated and the initial distance of the reactants was $\sqrt{x^2 + b^2}$, where $x=10 \text{ bohr}$ and the

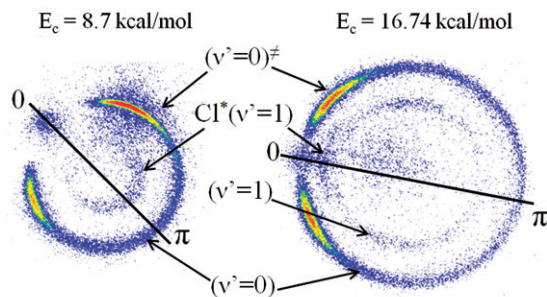


Figure 1. Two representative time-sliced raw images of the $\text{CH}_3(v=0)$ products at different collision energies. The state labelling ($v'=0$), ($v'=1$), ($v=0$) ‡ , and $[\text{Cl}^*(v'=1)]$ correspond to the correlated HCl vibrational states from Reactions (1), (2), (3) and (4), respectively. Some backgrounds are readily identified and subtracted out in data analysis.

impact parameter, b , was scanned from 0 to 7 bohr with a step size of 0.5 bohr. 5000 trajectories were computed at each b ; thus, the total number of trajectories was 75,000 for each collision energy. We have run QCTs at several collision energies in the 3.7–20.0 kcal/mol range. All the trajectories were integrated using 0.0726 fs integration step allowing a maximum of 20,000 time steps (~ 1.5 ps).

4. Results and discussion

4.1. Raw images and identification of reactions

Figure 1 presents two raw $\text{CH}_3(v=0)$ product images for illustration. Superimposed on the images are the relative velocity line with the forward (0°) and backward (π) directions indicated. Several distinct ring-like features are clearly displayed and can be readily identified on the basis of conservations of energy and momentum. The most intense feature, labelled as ($v'=0$), corresponds to Reaction (1) with $\Delta H_{rx} = 1.21$ kcal mol $^{-1}$. Adjacent to the outer-rim of this ring is a weak feature, labelled as ($v'=0$) ‡ , from the Reaction (3), where v_2 and v_4 are the two low-lying bend-modes with one quantum excitation energy of 4.38 kcal mol $^{-1}$ and 3.75 kcal mol $^{-1}$, respectively. The innermost circle in the higher E_c image, labelled as ($v'=1$), arises from the reaction of Reaction (2), $\Delta H_{rx} = 9.45$ kcal mol $^{-1}$. The remaining features on the two images, labelled as $[\text{Cl}^*(v'=1)]$, corresponds to Reaction (4), $\Delta H_{rx} = 6.93$ kcal mol $^{-1}$.

Two aspects of these images are worth noting. First, the raw images illustrate vividly the power of the time-sliced, velocity imaging technique, with which several different reactions and/or product channels can be interrogated simultaneously. Second, the

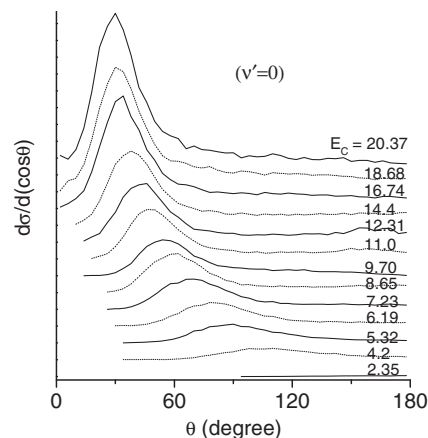


Figure 2. Measured product pair-correlated angular distributions for Reaction (1), $\text{Cl}(^2P_{3/2}) + \text{CH}_4(v=0) \rightarrow \text{CH}_3(v=0) + \text{HCl}(v'=0)$. The distributions have been normalized according to the excitation function shown in Figure 9. The number labels the collisional energy, E_c , in kcal mol $^{-1}$. For clarity, the distributions are shifted upward with increasing E_c , and only every other distribution is shown.

pair-correlated angular distributions of the spin-orbit excited Reaction (4), $[\text{Cl}^*(v'=1)]$, show a dramatic change from a broad backward/sideways distribution at $E_c = 8.7$ kcal mol $^{-1}$ to a forward peaking one at $E_c = 16.74$ kcal mol $^{-1}$. Interestingly, no image feature can be assigned to the $\text{HCl}(v'=0)$ coproducts, indicative of a highly inverted HCl vibrational state population when $\text{Cl}^*(^2P_{1/2})$ reacts with $\text{CH}_4(v=0)$. The absence of the signal from the $\text{HCl}(v'=0)$ product channel not only conforms our previous conclusion that the reactivity of $\text{Cl}^*(^2P_{1/2})$ atom toward methane is negligibly small at $E_c = 4.6$ kcal mol $^{-1}$ [50], but also extend the claim of a small $\text{HCl}(v'=0)$ yield to the higher E_c s.

4.2. Pair-correlated differential cross sections and their E_c -dependences

Similar images were acquired over a wide energy range from 2.4 kcal mol $^{-1}$ to 20.4 kcal mol $^{-1}$. After normalizing each individual $\text{CH}_3(v=0)$ image taken at different energy and correcting for the density-to-flux transformation [44,51], quantitative angular distribution of each distinct ring and its dependence on E_c can be deduced. The results for ($v'=0$), ($v'=1$), ($v=0$) ‡ , and $[\text{Cl}^*(v'=1)]$ are shown in Figures 2–5, respectively, where only the results of every other E_c are presented for clarity. A casual inspection of these series of distributions immediately reveals several remarkable observations. (i) For the ground state reaction (1),

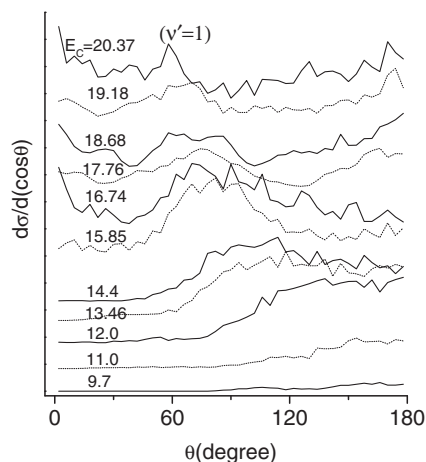


Figure 3. As Figure 2, but for Reaction (2), $\text{Cl}(^2P_{3/2}) + \text{CH}_4(v=0) \rightarrow \text{CH}_3(v=0) + \text{HCl}(v'=1)$.

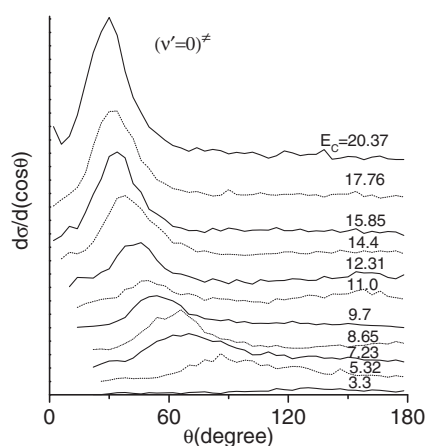


Figure 4. As Figure 2, but for Reaction (3), $\text{Cl}(^2P_{3/2}) + \text{CH}_4(v_2/v_4=1 \text{ or } v_b=1) \rightarrow \text{CH}_3(v=0) + \text{HCl}(v'=0)$.

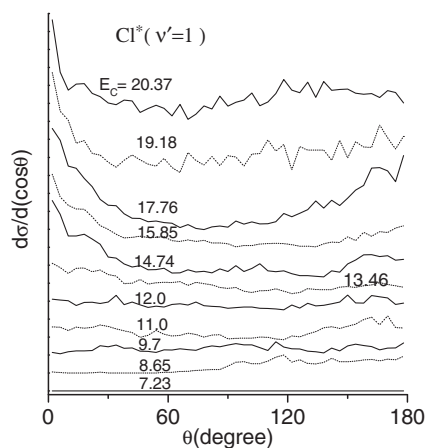


Figure 5. As Figure 2, but for Reaction (4), $\text{Cl}^*(^2P_{1/2}) + \text{CH}_4(v=0) \rightarrow \text{CH}_3(v=0) + \text{HCl}(v'=1)$.

Figure 2, the angular distribution is mainly backward at E_c near the threshold, but shifts to sideways-dominance at slightly higher E_c and continues evolving into sharply peaking distributions in the forward hemisphere with further increase in E_c . The distributions in the lower E_c portion ($E_c \leq 7.23 \text{ kcal mol}^{-1}$) agree very well with the previous study at low E_c regime [4]. Also worth noting is a clear intensity drop disfavoring forward-scattered products at E_c as high as 20 kcal mol^{-1} . Similar finding was noted in previous studies of reactions of Cl atom with CHD_3 [35,52] and CH_2D_2 [53], and is ascribed to be a characteristic feature in a direct reaction proceeds by the peripheral mechanism [4,9]. A peripheral reaction not only favours large impact parameter collisions, but also invokes significant impulsive energy release of recoiled products and thus restrains the products being scattered in the forward direction. The latter trait is distinct from the spectator-stripping mechanism [54], which has negligible impulsive release and thus yields an angular distribution peaking at 0° . (ii) The general pattern for the bend-excited reaction (3), Figure 4, appears strikingly similar to Reaction (1). Such a similarity strongly suggests that the two reactions proceed via a similar pathway. And (iii) the other product channel, $\text{HCl}(v'=1)$, from either the Reaction (2) (Figure 3) or the spin-orbit excited $\text{Cl}^*(^2P_{1/2})$ reaction (Figure 5, Reaction (4)) display distinct angular distributions from the above two reactions. While at lower E_c both reactions are backward dominant, at higher E_c the distributions for $[\text{Cl}^*(v'=1)]$ become forward-backward peaking and those for $(v'=1)$ also exhibit similar features with additional sideways structures. Clearly, the formation of $\text{HCl}(v'=1)$ from either spin-orbit ground $\text{Cl}(^2P_{3/2})$ or excited $\text{Cl}^*(^2P_{1/2})$ reactant proceeds through very different pathways and mechanisms from the two reactions yielding the $\text{HCl}(v'=0)$ products.

The enormous amounts of information embedded in Figures 2–5 can be summarized and more readily digested in a three-dimensional plot of $d\sigma/d(\cos\theta)$ as a function of both θ and E_c , as presented in Figure 6 for the four reactions. One notes immediately that the global patterns for the formation of $\text{HCl}(v'=0)$ from Reactions (1) and (3) are alike, and they are vastly different from the other two for the $\text{HCl}(v'=1)$ channels. We asserted previously [4,52,53] that the distinct ridge, spanning over a broad E_c range, and the clear cut-off angle against the forward scattered $\text{HCl}(v'=0)$ products can be regarded to the imprints of a direct reaction governed by peripheral dynamics. On the other hand, the pattern seen for the reaction (2) appears reminiscent of that reported previously in a resonance-mediated $\text{F} + \text{HD} \rightarrow \text{HF} + \text{D}$ reaction [55].

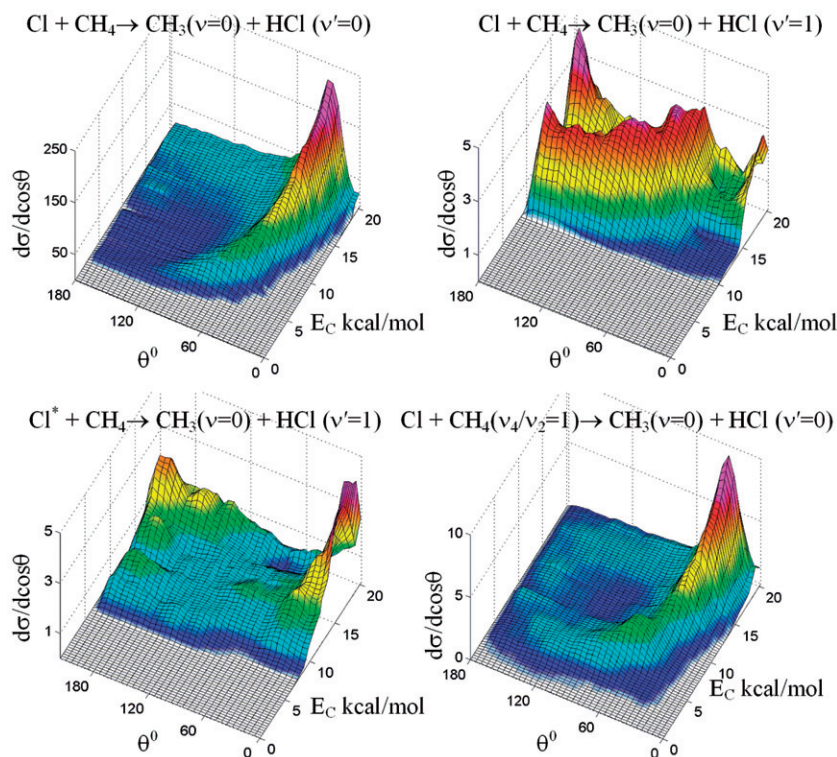


Figure 6. Three-dimensional plot of the experimental DCS $d\sigma/d(\cos\theta)$ as a function of θ and E_c , showing the evolution of the pair-correlated angular distributions with increasing collision energies for the four reactions as labelled.

Based on the pattern comparison and its contrast to that for the ground state reaction, we previously proposed [5,6] the existence of reaction (Feshbach) resonances in Reaction (2). Several recent theoretical investigations confirmed the proposition [56,57]. As to the pattern for the spin-orbit excited reactivity, we first note the dominance of forward-backward peaking features. Similar features were previously reported in two other non-adiabatic reactions: $F^*(^2P_{1/2}) + HD \rightarrow HF(v'=3) + D$ [58] and $Cl^*(^2P_{1/2}) + CH_2D_2 \rightarrow CHD_2(v=0) + HCl(v'=1)$ [53]. It was conjectured [53,58] that both non-adiabatic reactivity are mediated by resonances; the same interpretation is suggested for the present case. A very recent reduced dimensionality quantum scattering calculation on the spin-orbit non-adiabatic transitions in the present reaction also found resonance features [57]. Although the nature of the resonances can not be deciphered in that study because of the reduced dimensionality approximation, theory also found [57] that the spin-orbit excited reaction preferentially produced $HCl(v'=1)$, which is in excellent agreement with the present experimental finding as well as that in the previous $Cl^*(^2P_{1/2}) + CH_2D_2$ study [53]. Moreover, both experiment and theory strongly suggest a very active role of vibrations played in the

spin-orbit nonadiabatic transitions of this reaction [53,57,59,60]. Higher dimensionality quantum dynamics investigations will be particularly welcome to elucidate the nature of the resonances-mediated non-adiabatic reaction mechanism proposed here and elsewhere.

The QCT differential cross sections for $Cl + CH_4(v_b=0,1)$ at three collision energies are given in Figure 7. As E_c increases the systematic trend of shifting from backward to sideways and further into the forward hemisphere is apparent, which agrees well with the experimental results. At a fixed E_c the DCSs for the ground-state and bend-excited reactions resemble each other, which also corroborates very well with experimental findings. Also note that the reactivity of two bending-mode excitations, $v_2=1$ and $v_4=1$, are nearly identical.

To gain deeper insights into the shapes of DCS, Figure 8 presents the theoretical opacity function that measures the reaction probability as a function of impact parameters. Comparing Figure 8 with Figure 7, one notes a mirror-like behaviour of the two distributions: Small impact-parameter collisions yield backward scattered products and larger impact-parameter collisions lead to products at small scattering angles.

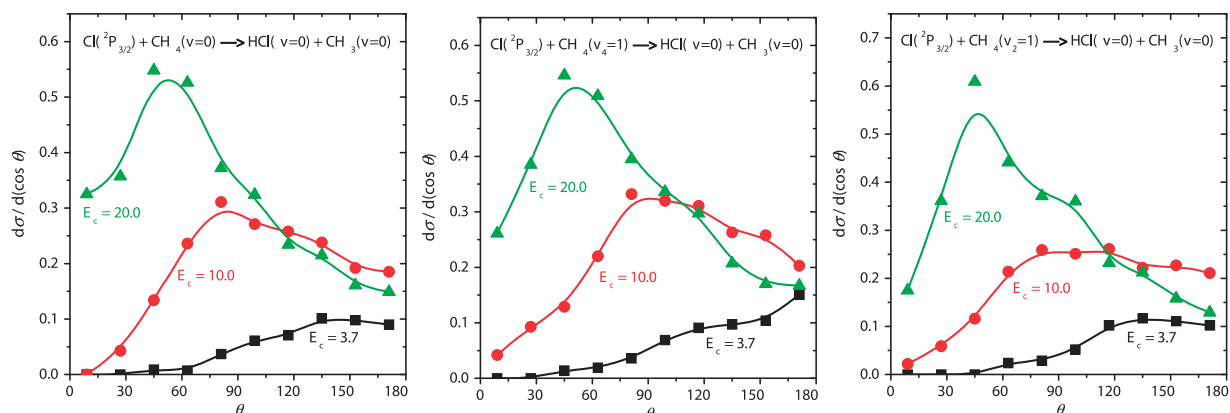


Figure 7. Computed angular distributions of the $\text{Cl}(^2P_{3/2}) + \text{CH}_4(v=0)$ and $\text{CH}_4(v_b=1)$ [$b=4, 2$] $\rightarrow \text{HCl}(v=0) + \text{CH}_3(v=0)$ reactions at collision energies of 3.7, 10.0, and 20.0 kcal mol^{-1} . The QCT calculations with and without zero-point energy constraint result basically in the same angular distributions, here the statistically more robust non-constrained results are presented. The vibrational state assignment for CH_3 was done as described in [49].

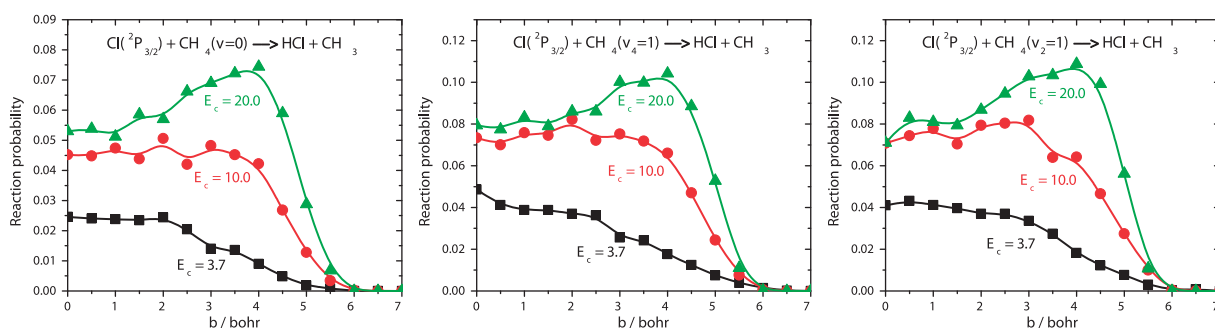


Figure 8. Computed reaction probabilities as a function of impact parameter for $\text{Cl}(^2P_{3/2}) + \text{CH}_4(v=0)$ and $\text{CH}_4(v_b=1)$ [$b=4, 2$] $\rightarrow \text{HCl}(\text{all states}) + \text{CH}_3(\text{all states})$ at collision energies of 3.7, 10.0, and 20.0 kcal mol^{-1} . The reaction probabilities are based on all the trajectories regardless the internal energy of the products.

Similar one-to-one correspondence between the DCS and the opacity function was observed in a previous reduced dimensionality quantum dynamics calculation of the $\text{Cl} + \text{CHD}_3$ reaction [52]. Such behaviour is anticipated for a direct reaction governed by the line-of-centres, hard-sphere type of collisions [54]. The way of the shape-change of the opacity function with E_c is entirely consistent with the notion of shifting the reaction mechanism from a rebound type at low E_c to peripheral at high E_c . The idea of a peripheral mechanism is based on the geometric consideration that the transferred H-atom, which is the reaction centre, is always sprouting away from the centre-of-mass of CH_4 . This site-specific reactivity leads to a simple approximation to the reactive zone of CH_4 reactant by an annulus [4,61], resulting in a higher reaction probability at larger impact parameter provided the collision energy is sufficiently high to surmount the centrifugally-shifted barrier to reaction.

In that regard, we note that the DCS calculated by QCT method at high E_c (Figure 7) is not as sharply peaking as the experimental results (Figure 2). The effects of quantum tunnelling through the centrifugal barrier may account for this discrepancy, although the zero-point energy issue cannot be completely ruled out.

4.3. Pair-correlated excitation functions

Integrating the normalized DCS for each E_c over the scattering angles θ , weighted by the solid-angle factor of $\sin\theta$, yields the normalized ICS. Figure 9 summarized the excitation functions of the four reactions. Since the four reactions involve different reactants, $\text{CH}_4(v=0)$, $\text{CH}_4(v_b=1)$, $\text{Cl}(^2P_{3/2})$, and $\text{Cl}(^2P_{1/2})$, the depicted excitation functions are not normalized to one another; only the E_c -dependences are of concern here. All excitation functions exhibit the typical behaviour of

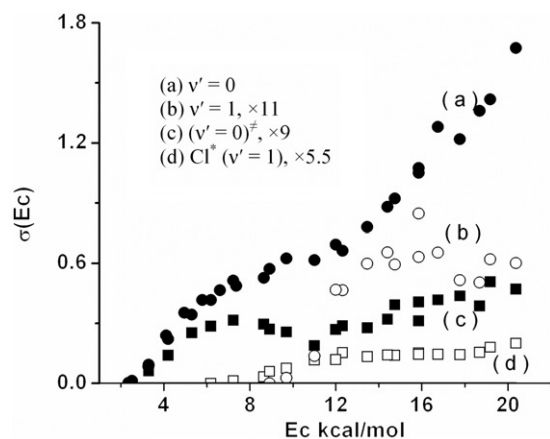


Figure 9. Measured relative excitation functions of the four reactions: (a) for Reaction (1), (b) for Reaction (2), (c) for Reaction (3), and (d) for Reaction (4).

an activated reaction. Yet, the E_c -dependences of the $\text{HCl}(v'=0)$ channel in both the $\text{Cl} + \text{CH}_4(v_b=0)$ and $\text{Cl} + \text{CH}_4(v_b=1)$ reaction, (a) and (c), respectively, indicate intriguing ‘dips’ around $E_c \sim 11 \text{ kcal mol}^{-1}$. While one might argue that the dip in (a) or Reaction (1) could be associated with the opening of the $\text{HCl}(v'=1)$ channel, i.e. (b) for Reaction (2), the same cannot be said for (c) because it involves bend-excited $\text{CH}_4(v_b=1)$ reactant, Reaction (3). Alternatively, vibrationally excited methyl radicals can be formed at these energies; unfortunately, their REMPI signals are too small to get reliable results. Further works will be needed to clarify the ‘dips’

In terms of the respective reaction thresholds, the ground state reaction (1) or (a) exhibits a clear onset at $E_c \sim 2.5 \text{ kcal mol}^{-1}$, which is somewhat lower than the theoretically calculated vibrationally adiabatic ground state barrier height of $3.4 \text{ kcal mol}^{-1}$ [43,62], indicative of the significance of tunnelling effects. Interestingly, the onset for the bend-excited reaction (3) or (c) occurs at the same E_c as the ground state reaction, in spite of the vibrational enhancement in reactivity in the post-threshold region [50]. Apparently, the extra bending energy ($\sim 4 \text{ kcal mol}^{-1}$) does not help the system surmount the barrier near the threshold, which is in sharp contrast to the stretch-excited reaction where the threshold drops to less than 1 kcal mol^{-1} [6,35]. The reactive onsets in forming the $\text{HCl}(v'=1)$ products are $9.5 \text{ kcal mol}^{-1}$ for (b) and $\sim 7.5 \text{ kcal mol}^{-1}$ for (d); both are in accord with the energetic expectations. The observation for (d) also implies that the spin-orbit non-adiabatic transition must take place prior to the transition state so that the extra energy of $\text{Cl}^*(^2P_{1/2})$ can facilitate the barrier crossing.

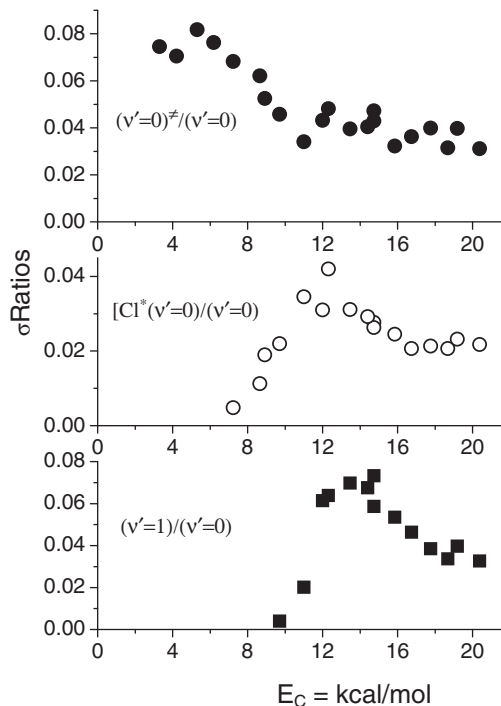


Figure 10. Measured reactivity ratios of Reaction (3), (4), and (2) to Reaction (1) are shown in the top, middle, and bottom panels, respectively. Presented in the top and middle panels are the observed signals, thus uncorrected for the relative reactant concentration factors (see text).

It is instructive to compare the relative reactivity of the four reactions. Plotted in Figure 10 are the ratios of the three minor reactions to the dominant ground-state reaction (1). The bottom panel indicates the HCl vibrational branchings, in concomitance with the probed $\text{CH}_3(v=0)$, as a function of E_c . Clearly, the reaction of $\text{Cl} + \text{CH}_4(v=0)$ produces mainly the ground-state product pair of $\text{CH}_3(v=0) + \text{HCl}(v'=0)$, i.e. a predominantly vibrational-adiabatic process. Similar conclusions were drawn experimentally for the reactions of $\text{Cl} + \text{CHD}_3(v=0)$ [35] and $\text{Cl} + \text{CH}_2\text{D}_2(v=0)$ [31,53]. Recent theoretical calculation also confirmed it [43]. The reactivity ratios shown in the upper two panels actually include the concentration factors of different reactants, i.e. $n^\# / n_0$ and $n_{\text{Cl}^*} / n_{\text{Cl}}$, respectively. Following the previous approach [38,39,50] by assuming an equal reactivity from the two bend-excited reactants ($v_2=1$ and $v_4=1$) that seems justified theoretically (Figure 7), the ordinate of the top panel should then multiply by ~ 30 to get the true cross-section ratio. The resulted $\sigma^\#(v'=0) / \sigma_0(v'=0)$ will then read 2.5 ± 1.0 at low E_c and drops to $\sim 1.3 \pm 1.0$ at high E_c . Despite the large error bar, which is mainly due to the estimated relative number densities of the bend-excited CH_4 in the beam, the

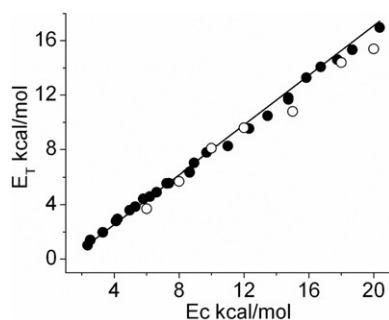


Figure 11. Dependences of the average kinetic energy release E_T for the $\text{Cl}(^2P_{3/2}) + \text{CH}_4(v=0) \rightarrow \text{CH}_3(v=0) + \text{HCl}(v'=0, 1)$ reaction on the initial collision energies. The solid dots are from experiment, the open circles from QCT, and the solid line is the prediction from a parameter-free kinematics model. The QCT calculations consider trajectories in which both HCl and CH_3 have classical vibrational energies greater than the corresponding zero-point energies. The vibrational state assignment for CH_3 was done as described in [49].

declining trend of the cross-section ratios with the increase of E_c is clear. The reported ratios are in accord with the previous result of 2–4 at $E_c = 4.6 \text{ kcal mol}^{-1}$ [50], and with the enhancement factor of 3 ± 1 at $E_c = 3.7 \text{ kcal mol}^{-1}$ from Zare's group [27]. Similar bend-excited enhancement factors were reported for the $\text{Cl} + \text{CHD}_3(v_b=1)$ [35] and $\text{Cl} + \text{CH}_2\text{D}_2(v_b=1)$ [53] reactions. All experimental results also agree very well the QCT results of this study, which give ratios of 2–3 over this energy range. As to the spin-orbit excited reaction (the middle panel), the relative population of $\text{Cl}^*(^2P_{1/2})$ in the beam, $n_{\text{Cl}^*}/n_{\text{Cl}}$, was not measured in this study. We expect it to be less than 1/2 (i.e. the relative degeneracy factors of the excited $^2P_{1/2}$ to the ground $^2P_{3/2}$ state). With this caveat, the relative reactivity of $\text{Cl}^*(^2P_{1/2})$ towards CH_4 appears to be around 4–8% (the lower bound). Similar magnitudes were estimated previously for $\text{Cl}^* + \text{CH}_2\text{D}_2$ [53], and found in a recent reduced dimensionality quantum dynamics calculation [57].

4.4. Product kinetic energy release

Figure 11 shows the dependences of the average kinetic energy release E_T of the $\text{Cl} + \text{CH}_4(v=0) \rightarrow \text{HCl}(v') + \text{CH}_3(v=0)$ reaction. The solid and open circles are the experimental and QCT results, respectively. Both indicate that E_T rises linearly with E_c . The slight discrepancy between theory and experiment could arise from the probe-bias mentioned in Section 2. Also shown in the figure is the prediction from a mere consideration of kinematics constraint. The reaction is essentially a heavy + light-heavy system, involving

H-atom transfer from the CH_3 -moiety to the attacking Cl-atom. For such a mass combination of an endothermic reaction, a simple kinematics model [54] predicts the average kinetic energy release as $E_T = (E_c - \Delta H_{rx}) \cos^2 \beta$. Here, ΔH_{rx} is the endothermicity and β is the skew angle, $\cos^2 \beta = m_A m_C / m_{AB} m_{BC}$, for the $\text{A} + \text{BC} \rightarrow \text{AB} + \text{C}$ reaction. As is seen, the model prediction reproduces the experimental and QCT data over a wide range of E_c . Since no adjustable parameter is invoked in the model, such a remarkable agreement provides a compelling evidence for the dominance of kinematics in governing the product kinetic energy release. In other words, kinetic energy is nearly conserved for a light-atom transfer reaction. This conclusion reinforces our previous findings for the $\text{Cl} + \text{CHD}_3$ [52] and $\text{Cl} + \text{CH}_2\text{D}_2$ [53] reactions.

5. Conclusions

To summarize, some key issues about the $\text{Cl} + \text{CH}_4$ reaction dynamics are addressed in this work, from which several conclusions can be drawn. First, the comparisons between experiment and theory are made on both ICS and DCS, for both ground state and bend-excited CH_4 reactants, over the energy range from reaction threshold up to 20 kcal mol^{-1} . This is a rather extensive set of data. The general agreement found in this work, as well as on the other dynamical aspects reported elsewhere [43], gives us the confidence in the quality and the accuracy of the newly developed *ab initio* PES [43] for further dynamical investigations. Some small discrepancies are noted, which call for quantum dynamics investigations in the future. Second, the $\text{HCl}(v'=0)$ products in Reactions (1) and (3) are formed by a direct abstraction process. The underlying mechanism shifts from a typical rebound type at low E_c to a peripheral dynamics at high E_c . Third, the formation of $\text{HCl}(v'=1)$ products, either Reactions (2) or (4), proceeds via different pathways from the above $\text{HCl}(v'=0)$ channels. The observed patterns in $d\sigma/d(\cos\theta)$ as a function of both θ and E_c show distinct characteristics of complex-forming reactions. Hence, two most common types of chemical reactions, direct and indirect, coexist in this benchmark polyatomic reaction. The tentative conclusion of resonance-mediated spin-orbit reactivity is intriguing and deserves further studies in the future.

Acknowledgements

K.L. thanks the National Science Council of Taiwan, Academia Sinica, and the Air Force Office of Scientific

Research (grant No. AOARD 124020) for financial support. G.C. thanks the National Science Foundation (CHE-0625237) and J.M.B. thanks the Department of Energy (DE-FG02-97ER14782) for financial support.

References

- [1] M.S. Zahriser, B.M. Berquist and F. Kaufman, *Int. J. Chem. Kinet.* **10**, 15 (1978).
- [2] A.R. Ravishankara and P.H. Wine, *J. Chem. Phys.* **72**, 25 (1980).
- [3] J.S. Pilgrim, A. McIlroy and C.A. Taatjes, *J. Phys. Chem. A* **101**, 1873 (1997).
- [4] J. Zhou, B. Zhang, J.J. Lin and K. Liu, *Mol. Phys.* **103**, 1757 (2005).
- [5] B. Zhang and K. Liu, *J. Chem. Phys.* **122**, 101102 (2005).
- [6] H. Kawamata and K. Liu, *J. Chem. Phys.* **133**, 124304 (2010).
- [7] T.N. Truong, D.G. Truhlar, K.K. Baldrige, M.S. Gordon and R. Steckler, *J. Chem. Phys.* **90**, 7137 (1989).
- [8] D. Troya, J. Millan, I. Banos and M. Gonzalez, *J. Chem. Phys.* **117**, 5730 (2002).
- [9] X. Wang, M. Ben-Nun and R.D. Levine, *Chem. Phys.* **197**, 1 (1995).
- [10] G. Nyman, H.-G. Yu and R.B. Walker, *J. Chem. Phys.* **109**, 5896 (1998).
- [11] H.-G. Yu and G. Nyman, *J. Chem. Phys.* **110**, 7233 (1999).
- [12] W.T. Duncan and T.N. Truong, *J. Chem. Phys.* **103**, 9642 (1995).
- [13] J. Espinosa-Garcia and J.C. Corchado, *J. Chem. Phys.* **105**, 3517 (1996).
- [14] J. Sanson, J.C. Corchado, C. Rangel and J. Espinosa-Garcia, *J. Chem. Phys.* **124**, 074312 (2006).
- [15] D. Troya and P.J.E. Weiss, *J. Chem. Phys.* **124**, 074313 (2006).
- [16] S.T. Banks and D.C. Clary, *Phys. Chem. Chem. Phys.* **9**, 933 (2007).
- [17] S. Rudic, C. Murray, J.N. Harvey and A.J. Orr-Ewing, *J. Chem. Phys.* **120**, 186 (2004).
- [18] J.C. Corchado, D.G. Truhlar and J. Espinosa-Garcia, *J. Chem. Phys.* **112**, 9375 (2002).
- [19] S. Yoon, S. Henton, A.N. Zikovic and F.F. Crim, *J. Chem. Phys.* **116**, 10744 (2002).
- [20] S. Yoon, R.J. Holiday, E.L. Sibert III and F.F. Crim, *J. Chem. Phys.* **119**, 9568 (2003).
- [21] S. Yoon, R.J. Holiday and F.F. Crim, *J. Chem. Phys.* **119**, 4755 (2003).
- [22] R.J. Holiday, C.H. Kwon, C.J. Annesley and F.F. Crim, *J. Chem. Phys.* **125**, 133101 (2006).
- [23] C.J. Annesley, A.E. Berke and F.F. Crim, *J. Phys. Chem. A* **112**, 9448 (2008).
- [24] W.R. Simpson, T.P. Rakitzis, S.A. Kandel, T. Lev-On and R.N. Zare, *J. Phys. Chem.* **100**, 7938 (1996).
- [25] W.R. Simpson, T.P. Rakitzis, S.A. Kandel, A.J. Orr-Ewing and R.N. Zare, *J. Phys. Chem.* **103**, 7313 (1995).
- [26] H.A. Bechtel, J.P. Camden, D.J. Ankeny Brown and R.N. Zare, *J. Chem. Phys.* **120**, 5096 (2004).
- [27] H.A. Bechtel, J.P. Camden, D.J. Ankeny Brown, M.R. Martin, R.N. Zare and K. Vodopyanov, *Angew. Chem. Intern. Ed.* **44**, 2382 (2005).
- [28] Z.H. Kim, H.A. Bechtel and R.N. Zare, *J. Am. Chem. Soc.* **123**, 12714 (2001).
- [29] H.A. Bechtel, Z.H. Kim, J.P. Camden and R.N. Zare, *J. Chem. Phys.* **120**, 791 (2004).
- [30] H. Kawamata, S. Tauro and K. Liu, *Phys. Chem. Chem. Phys.* **10**, 4378 (2008).
- [31] J. Riedel, S. Yan and K. Liu, *J. Phys. Chem. A* **113**, 14270 (2009).
- [32] J. Riedel and K. Liu, *J. Phys. Chem. A* **113**, 4249 (2009).
- [33] S. Yan, Y.-T. Wu and K. Liu, *Phys. Chem. Chem. Phys.* **9**, 250 (2007).
- [34] S. Yan and K. Liu, *Chinese J. Chem. Phys.* **20**, 333 (2007).
- [35] S. Yan, Y.-T. Wu, B. Zhang, X.-F. Yue and K. Liu, *Science* **316**, 1723 (2007).
- [36] S. Yan, Y.-T. Wu and K. Liu, *Proc. Natl. Acad. Sci. USA* **105**, 12667 (2008).
- [37] F. Wang, J.-S. Lin and K. Liu, *Science* **331**, 900 (2011).
- [38] G. Czako, Q. Shuai, K. Liu and J.N. Bowman, *J. Chem. Phys.* **133**, 131101 (2010).
- [39] F. Wang and K. Liu, *J. Phys. Chem. Lett.* **2**, 1421 (2011).
- [40] W. Zhang, H. Kawamata and K. Liu, *Science* **325**, 303 (2009).
- [41] B. Zhang and K. Liu, *J. Phys. Chem. A* **109**, 6791 (2005).
- [42] F. Wang and K. Liu, *Chem. Sci.* **1**, 126 (2010).
- [43] G. Czako and J.M. Bowman, *Science* **334**, 343 (2011).
- [44] J.J. Lin, J. Zhou, W. Shiu and K. Liu, *Rev. Sci. Instrum.* **74**, 2495 (2003).
- [45] J.J. Lin, J. Zhou, W. Shiu and K. Liu, *Science* **300**, 966 (2003).
- [46] W. Shiu, J.J. Lin and K. Liu, *Phys. Rev. Lett.* **92**, 103201 (2004).
- [47] W. Shiu, J.J. Lin, K. Liu, M. Wu and D.H. Parker, *J. Chem. Phys.* **120**, 117 (2004).
- [48] W.L. Hase, *Encyclopedia of Computational Chemistry* (Wiley, New York, 1998), pp. 399–407.
- [49] G. Czako and J.M. Bowman, *J. Chem. Phys.* **131**, 244302 (2009).
- [50] J. Zhou, J.J. Lin, B. Zhang and K. Liu, *J. Phys. Chem. A* **108**, 7832 (2004).
- [51] D.M. Sonnenfroh and K. Liu, *Chem. Phys. Lett.* **176**, 183 (1991).
- [52] G. Nyman, J. Zhou, B. Zhang and K. Liu, *Isr. J. Chem.* **47**, 1 (2007).
- [53] Y.-T. Wu and K. Liu, *J. Chem. Phys.* **129**, 154302 (2008).
- [54] R.D. Levine and R.B. Bernstein, *Molecular Reaction Dynamics and Chemical Reactivity* (Oxford University Press, Oxford, 1987), pp. 10–11.

- [55] R.T. Skodje, D. Skouteris, D.E. Manolopoulos, S.-H. Lee, F. Dong and K. Liu, *Phys. Rev. Lett.* **85**, 1206 (2000).
- [56] R. Martinez, M. Gonzalez, P. Defazio and C. Petrongolo, *J. Chem. Phys.* **127**, 104302 (2007).
- [57] S.M. Rimmert, S.T. Banks, J.N. Harvey, A.J. Orr-Ewing and D.C. Clary, *J. Chem. Phys.* **134**, 204311 (2011).
- [58] S.-H. Lee, F. Dong and K. Liu, *Faraday Discuss* **127**, 49 (2004).
- [59] B. Retail, J.K. Pearce, S.J. Greaves, R.A. Rose and A.J. Orr-Ewing, *J. Chem. Phys.* **128**, 184303 (2008).
- [60] R.A. Rose, S.J. Greaves and A.J. Orr-Ewing, *Mol. Phys.* **108**, 981 (2010).
- [61] J.J. Valentini, *J. Phys. Chem. A* **106**, 5745 (2002).
- [62] G. Czako and J.M. Bowman, *J. Chem. Phys.* **136**, 044307 (2012).